

Aberystwyth University

When is a surface foam-phobic or foam-philic?

Teixeira, Miguel A. C.; Arscott, Steve; Cox, Simon; Teixeira, Paulo I. C.

Published in:
Soft Matter

DOI:
[10.1039/C8SM00310F](https://doi.org/10.1039/C8SM00310F)

Publication date:
2018

Citation for published version (APA):

Teixeira, M. A. C., Arscott, S., Cox, S., & Teixeira, P. I. C. (2018). When is a surface foam-phobic or foam-philic? *Soft Matter*, 14, 5369-5382. <https://doi.org/10.1039/C8SM00310F>

General rights

Copyright and moral rights for the publications made accessible in the Aberystwyth Research Portal (the Institutional Repository) are retained by the authors and/or other copyright owners and it is a condition of accessing publications that users recognise and abide by the legal requirements associated with these rights.

- Users may download and print one copy of any publication from the Aberystwyth Research Portal for the purpose of private study or research.
- You may not further distribute the material or use it for any profit-making activity or commercial gain
- You may freely distribute the URL identifying the publication in the Aberystwyth Research Portal

Take down policy

If you believe that this document breaches copyright please contact us providing details, and we will remove access to the work immediately and investigate your claim.

tel: +44 1970 62 2400
email: is@aber.ac.uk

When is a surface foam-phobic or foam-philic?

Miguel A. C. Teixeira*

*Department of Meteorology, University of Reading
Earley Gate, PO Box 243, Reading RG6 6BB, United Kingdom**

Steve Arscott[†]

*Institut d'Electronique, de Microélectronique et de Nanotechnologie (IEMN)
CNRS UMR8520, The University of Lille
Cité Scientifique, Avenue Poincaré, 59652 Villeneuve d'Ascq, France[†]*

Simon J. Cox[‡]

*Department of Mathematics, Aberystwyth University
Aberystwyth, Ceredigion, SY23 3BZ, United Kingdom[‡]*

Paulo I. C. Teixeira[§]

*ISEL – Instituto Superior de Engenharia de Lisboa, Instituto Politécnico de Lisboa
Rua Conselheiro Emídio Navarro 1, 1959-007 Lisbon, Portugal and
Centro de Física Teórica e Computacional,
Faculdade de Ciências da Universidade de Lisboa
Campo Grande, Edifício C8, 1749-016 Lisbon, Portugal[§]*

(Dated: 15 September 2017)

Abstract

By integrating the Young-Laplace equation, including the effects of gravity, we have calculated the equilibrium shape of the two-dimensional Plateau borders along which a vertical soap film contacts two flat, horizontal solid substrates of given wettability. We show that the Plateau borders, where most of a foam's liquid resides, can only exist if the values of the Bond number Bo and of the liquid contact angle θ_c lie within certain domains in (θ_c, Bo) space: under these conditions the substrate is foam-philic. For values outside these domains, the substrate cannot support a soap film and is foam-phobic. In other words, on a substrate of a given wettability, only Plateau borders of a certain range of sizes can form. For given (θ_c, Bo) , the top Plateau border can never have greater width or cross-sectional area than the bottom one. Moreover, the top Plateau border cannot exist in a steady state for contact angles above 90° . Our conclusions are validated by comparison with both experimental and numerical (Surface Evolver) data. We conjecture that these results will hold, with slight modifications, for non-planar soap films and bubbles. Our results are also relevant to the motion of bubbles and foams in channels, where the friction force of the substrate on the Plateau borders plays an important role.

PACS numbers: 83.80.Iz, 82.70.Rr

*Electronic address: m.a.teixeira@reading.ac.uk

†Electronic address: steve.arscott@iemn.univ-lille1.fr

‡Electronic address: foams@aber.ac.uk

§Electronic address: piteixeira@fc.ul.pt

I. INTRODUCTION

The wetting of a solid by a liquid – where the liquid will spread into a sheet or break up into droplets when placed onto the solid – is ubiquitous in nature as well as having practical importance in industry [1]. Wetting behaviour can be conveniently described in terms of the contact angle θ_c at which the liquid-vapour interface meets the solid-liquid interface: if $\theta_c = 0$ the liquid is said to completely (or perfectly) wet the solid, whereas if $0 < \theta_c \leq \pi/2$ wetting is only partial. Contact angles greater than $\pi/2$ correspond to drying (or de-wetting) of the solid by the liquid. If, as is often the case in practice, the liquid is water-based, a surface that is wetted ($0 \leq \theta_c \leq \pi/2$) is called hydrophilic, and one that is not ($\pi/2 < \theta_c \leq \pi$) hydrophobic. If θ_c is greater than about $5\pi/6$ (150°) there is only a very small area of contact between liquid and solid: essentially the liquid forms an almost spherical droplet that may, e.g., under the effect of gravity, roll off the solid, which is then termed superhydrophobic. Superhydrophobicity is a topic of much current research: see, e.g., [2–4] for reviews.

In confined foams, which include most real-life foams, there are, in addition to the usual bulk Plateau borders at which three (or more, in a wet foam) soap films meet, Plateau borders where the films meet the confining walls. These surface Plateau borders are bounded by the wall and (in fairly dry foams) by two curved liquid-vapour interfaces, see figure 1. These interfaces will, of course, meet the wall at the liquid contact angle θ_c . The question thus arises: what is the shape of a Plateau border of a given size (i.e., volume in 3D, area in 2D) on a surface of a given wettability? Or, in other words, when is a solid surface capable of supporting a foam, i.e. is the surface ‘foam-phobic’ or ‘foam-philic’? This is of paramount importance for assessing, e.g., the effectiveness of firefighting foams on different substrates, or the adequacy of containers for certain foamy foodstuffs.

In an earlier paper, we calculated the shape of a 2D surface Plateau border around a bubble sitting on a perfectly-wetting substrate in zero gravity [5]. This was later extended to 3D and a (fairly small but) finite contact angle [6], and to include the effect of gravity [7]. More recently, we calculated the equilibrium shape of the axially symmetric meniscus along which a bubble contacts a flat *liquid* surface [8]. Here we return to solid surfaces of variable wettability, but consider first the simpler case of a planar film spanning a gap between two parallel, flat substrates (a rectangular slit). The film and its associated surface

Plateau borders are thus effectively 2D (slab-symmetric): see figure 1.

Most of a foam’s liquid is contained within the network of Plateau borders. It is clear from the curvature of the Plateau border interfaces that the liquid is at lower pressure than the gas in the bubbles; indeed the interfacial curvature is set by this pressure difference and so, at the same height in a foam, the liquid in the bulk and surface Plateau borders will have the same pressure. As a consequence of their different shapes, however, the surface Plateau border (with one of its interfaces in contact with the planar wall) will have greater volume [9]. Thus, per unit length, the surface Plateau borders carry a disproportionately large amount of a foam’s liquid, and therefore understanding their shape and stability is important. Moreover, as a foam moves, it is the surface Plateau borders that drag along the substrate and set one of the important time-scales for foam dynamics [10].

This paper is organised as follows: in section II we describe our experimental method for measuring Plateau border shapes. These shapes can be found analytically for arbitrary gravity and liquid contact angle, which we do by solving the Young-Laplace equation in section III. We then derive the ranges of parameters for which such Plateau borders may exist, which is a necessary condition to form a foam on a surface of given wettability. An alternative method to find Plateau border shapes from numerical energy minimisation, using the Surface Evolver software, is described in section IV. Then in section V we compare the predictions of our analytical solution with experimental results, as well as with the fully numerical Surface Evolver solution. Finally, we conclude in section VI.

II. EXPERIMENTAL PROCEDURE

The film-surface wetting experiments were performed in a dust-free, controlled environment, using a class ISO 5/7 cleanroom, which ensures that the temperature (T) and relative humidity (RH) remain within the following ranges: $T = 20 \pm 0.5^\circ\text{C}$ and $RH = 45 \pm 2\%$. The data were gathered using a contact angle meter (GBX Scientific Instruments, France). A commercially-available surfactant solution (Pustefix, Germany) was employed to generate stable soap films for the experiments. This solution is a mixture of water, glycerol, and an organosulfate. The surface tension and the density of the solution have previously been measured to be $28.2 \pm 0.3 \text{ mJm}^{-2}$ and 997.8 kgm^{-3} [11].

Five different solid surfaces were used in the experiments, the properties of which are col-

lected in Table I. These five surfaces were prepared to ensure a range of wetting properties (with respect to the surfactant solution) from hydrophilic (low contact angle) to hydrophobic (high contact angle). A hydrophilic surface was prepared by chemically oxidising a commercial p-type ($5 - 10 \text{ } \Omega\text{cm}$) polished silicon wafer (Siltronix, France) in 65% nitric acid, thus creating a thin silicon oxide layer having a thickness of approximately 1 nm [12] (surface 1). Three intermediate wetting surfaces were fabricated from a commercial polished silicon wafer (roughness $< 1 \text{ nm}$) coated with a thin amorphous fluorocarbon (FC) layer [13] – referred to here as ‘teflonised polished silicon’ (surface 2); a 1 mm thick polydimethylsiloxane ‘PDMS’ elastomer block (1:10 PDMS Sylgard 184 Dow Corning) moulded in a dish (surface 3); and a ‘teflonised rough silicon’ surface made by depositing the thin amorphous FC on the unpolished rear side of a commercial silicon wafer of roughness $\approx 1 \text{ } \mu\text{m}$ (surface 4). A hydrophobic surface was prepared by coating ‘black silicon’, prepared using a Bosch® process etch under certain plasma conditions [14], with an FC layer – this is referred to here as ‘teflonised black silicon’ (surface 5). The FC layer was deposited by exposure of the surfaces (both silicon and black silicon) to a C_4F_8 plasma (Surface Technology Systems Ltd, UK), which resulted in the deposition of a thin (a few tens of nanometres) film of amorphous fluoropolymer on the surface of both the silicon and the black silicon. The teflonised black silicon was verified to be superhydrophobic: its wetting contact angle to water droplets was measured to be $154.5 \pm 2.4^\circ$ with near-zero contact angle hysteresis. The wetting contact angle of the surfactant solution was measured on each surface using the contact angle meter (see table I) and the results are consistent with previous measurements [11]. Figure 2 shows photographs of droplets of the surfactant solution on four of the five different surfaces described above.

A schematic diagram of the experimental setup and the working principle is shown in figure 3. It contains an in-house microfluidic tool which has been created specifically for the experiments. The tool incorporates two main elements: a microfluidic reservoir and a deformable ring, made of a loop of capillary tube. The role of the microfluidic reservoir is to increase the lifetime of the liquid film sufficiently to allow the formation of a stable Plateau border (see figure 3b). The lifetime of the liquid film was approximately 30 s in the current setup, which was sufficient to create a stable Plateau border and photograph it. An unwanted side-effect is that there is gravity-driven drainage from the reservoir towards the Plateau border, so that its volume increases during the experiment.

The role of the deformable loop is threefold: (i) to support a stable liquid film connected to the reservoir; (ii) to be thin enough so as not to perturb the Plateau border shape, e.g., thickness of loop very much less than the Plateau border dimensions h and b (see figure 3b); and (iii) the loop should be deformable to enable the formation of a long, stable Plateau border across the surface. Indeed, this deformability – leading to a long, voluminous Plateau border – combats the effect of drainage from the reservoir. The radius R of the deformable loop in the current setup is ≈ 1 cm.

We bring the tool containing the liquid film (figure 3a – ‘up’ position) carefully into contact with a small droplet resting on the specific surface under test (figure 3b – ‘down’ position) in the contact angle meter. Upon contact, and allowing the loop to be slightly deformed as shown in figure 3b, a long stable Plateau border is formed along the surface, over a length of about 1 cm, which can be photographed (side view in figure 3b) using the contact angle meter.

Figure 4 shows the practical components of the microfluidic tool. The reservoir is contained within capillary slots with a width and depth of ≈ 650 μm and a length of 6 mm (there are 14 on the tool, holding a total liquid volume of about 35 μl) made of ABS plastic. The loop which supports the liquid film is made of polyimide-coated capillary tubing (Molex, USA) having an outside diameter of 90 μm .

In the current setup it is very difficult to have the deformed loop perfectly perpendicular to the camera – this is visible at the top of the Plateau borders in the photographs (see figure 11). Moreover, as the loop is deliberately not rigid, the attached film can vibrate. A rough estimation of the soap film vibration frequency f (first mode) of a circular loop can be made by using $f = (1/2\pi)\sqrt{\gamma/\pi\rho R^2t}$, where γ , ρ and t are the soap film surface tension, density and thickness, and R is the loop radius. Taking t to be 1 μm and the values given in the text for the other quantities, one can estimate $f \approx 50$ Hz. In some cases, the amplitude of such oscillations can be of the order of millimetres [16]. This effect can contribute to blur in the photographs (low lighting – longer shutter times) at the top of the Plateau border. Another source of experimental error is non-perfect surfaces, which is apparent from the fact that the contact angles are not always equal on the left and on the right of the Plateau borders. This is inevitable despite care (e.g., working in a cleanroom in this case – surface preparation, storage and measurements): there are defects and contamination that cause wetting to be asymmetrical.

Finally, note that this setup only allows us to measure the Plateau border at the bottom substrate, not at the top one.

III. ANALYTICAL THEORY

The Young-Laplace law for the 2D (i.e., slab-symmetric) liquid surfaces bounding a Plateau border at a flat substrate (see figure 5a) can be written [17]:

$$\left[1 + \left(\frac{dx}{dz}\right)^2\right]^{-3/2} \frac{d^2x}{dz^2} = -\frac{\Delta p}{\gamma}, \quad (1)$$

where z is height measured from the substrate, x is the distance measured horizontally from the plane of symmetry (the plane of the 2D film), $\Delta p(z)$ is the pressure difference across the liquid surface at each height, and γ is the surface tension of the liquid.

Our aim is to solve equation (1) for one of the surfaces bounding each of the top and bottom Plateau borders of a 2D vertical film spanning the gap between two flat, horizontal substrates. Naturally, the other Plateau border surface is mirror-symmetric with respect to $x = 0$. The Plateau borders are slab-symmetric and in hydrostatic equilibrium. It is convenient to choose a definition of Δp that, by default, makes x predominantly positive in the most common situations. This is $\Delta p = p_b - p_a$, where p_b is the pressure inside the Plateau border (i.e., within the liquid) and p_a is the atmospheric pressure outside the Plateau border (assumed to be constant).

We shall start by considering the bottom Plateau border. Since p_b is assumed to be in hydrostatic equilibrium, we have

$$\Delta p = p_b - p_a = p_{b0} - p_a - \rho g z, \quad (2)$$

where p_{b0} is the pressure inside the Plateau border at the substrate ($z = 0$), g is the gravitational acceleration, and ρ is the density of the liquid inside the Plateau border (in our case water).

Additionally, we introduce the convenient change of variables given by

$$\frac{dx}{dz} = -\cot \theta \quad \Rightarrow \quad \frac{d^2x}{dz^2} = \operatorname{cosec}^2 \theta \frac{d\theta}{dz}, \quad (3)$$

where θ is the angle of inclination of the film surface (see figure 5a). Using equations (2) and (3), equation (1) becomes

$$\sin \theta \frac{d\theta}{dz} = \frac{p_a - p_{b0}}{\gamma} + \frac{\rho g z}{\gamma}. \quad (4)$$

This equation can be straightforwardly solved for θ , yielding

$$\cos \theta(z) = \cos \theta_c - \frac{p_a - p_{b0}}{\gamma} z - \frac{\rho g}{2\gamma} z^2, \quad (5)$$

where the integration has been carried out from the base of the Plateau border, $z = 0$, where $\theta = \theta_c$, to a generic height z . By definition, θ_c is the contact angle of the liquid with the underlying solid substrate, and varies in the interval $0 < \theta_c < \pi$. If equation (4) is instead integrated from $z = 0$ to the top of the Plateau border $z = h$, where it is assumed that the film is vertical (i.e., $\cos \theta = 0$, so $\theta = \pi/2$), this provides a definition for the pressure term on the right-hand side of the solution, equation (5), which allows us to eliminate this term:

$$\frac{p_a - p_{b0}}{\gamma} = \frac{1}{h} \cos \theta_c - \frac{\rho g h}{2\gamma}. \quad (6)$$

Equation (5) can now be expressed entirely in terms of z , h and θ_c , as follows:

$$\cos \theta(z) = \cos \theta_c \left(1 - \frac{z}{h}\right) + \frac{\rho g z}{2\gamma} (h - z). \quad (7)$$

This equation can be written more simply if z is made dimensionless by scaling it by h , $z' = z/h$, and a Bond number is defined as $\text{Bo} = \rho g h^2 / \gamma$. In terms of these quantities, equation (7) can be rewritten as

$$\cos \theta(z') = (1 - z') \left(\cos \theta_c + \frac{\text{Bo}}{2} z' \right). \quad (8)$$

To obtain x as a function of z , we now go back to the definition of dx/dz . Further defining $x' = x/h$, it follows that

$$\frac{dx'}{dz'} = \frac{dx}{dz} = -\cot \theta = -\frac{\cos \theta}{\sqrt{1 - \cos^2 \theta}}. \quad (9)$$

Using equation (8), equation (9) can be rewritten as

$$\frac{dx'}{dz'} = -\frac{(1 - z') \left(\cos \theta_c + \frac{\text{Bo}}{2} z' \right)}{\left[1 - (1 - z')^2 \left(\cos \theta_c + \frac{\text{Bo}}{2} z' \right)^2 \right]^{1/2}}. \quad (10)$$

Noting again that at the top of the Plateau border $x'(z = h) = x'(z' = 1) = 0$, equation (10) can be integrated between a generic z' and $z' = 1$, yielding

$$x'(z') = \int_{z'}^1 \frac{(1 - z'') \left(\cos \theta_c + \frac{\text{Bo}}{2} z'' \right)}{\left[1 - (1 - z'')^2 \left(\cos \theta_c + \frac{\text{Bo}}{2} z'' \right)^2 \right]^{1/2}} dz'' \quad (\text{bottom PB}). \quad (11)$$

This equation gives the shape of the right-hand surface bounding the bottom Plateau border (between $z' = 0$ and $z' = 1$). The shape of the top Plateau border is then immediately obtained by reversing the sign of g in equation (2) and following through the above derivation, with the result

$$x'(z') = \int_{z'}^1 \frac{(1 - z'') \left(\cos \theta_c - \frac{\text{Bo}}{2} z'' \right)}{\left[1 - (1 - z'')^2 \left(\cos \theta_c - \frac{\text{Bo}}{2} z'' \right)^2 \right]^{1/2}} dz'' \quad (\text{top PB}). \quad (12)$$

Note that, while the meaning of x' remains unchanged, in this case z' is a dimensionless height measured as positive downwards from the top substrate.

Another relevant quantity is the area delimited by the Plateau border cross-section. This is defined as

$$A = 2 \int_0^h x dz = 2 [zx]_0^h - 2 \int_0^h z \frac{dx}{dz} dz = -2 \int_0^h z \frac{dx}{dz} dz, \quad (13)$$

where the second equality results from integrating by parts, and the third equality follows from the fact that at the top of the Plateau border $x(z = h) = 0$. The factor of 2 in equation (13) accounts for the fact that the Plateau border surfaces are symmetric. Defining a dimensionless area as $A' = A/h^2$, this is given, from equation (13), by

$$A' = -2 \int_0^1 z' \frac{dx'}{dz'} dz'. \quad (14)$$

Using equation (10), equation (14) for the bottom Plateau border can be written explicitly as

$$A' = 2 \int_0^1 \frac{z'(1 - z') \left(\cos \theta_c + \frac{\text{Bo}}{2} z' \right)}{\left[1 - (1 - z')^2 \left(\cos \theta_c + \frac{\text{Bo}}{2} z' \right)^2 \right]^{1/2}} dz' \quad (\text{bottom PB}), \quad (15)$$

and the equivalent result for the top Plateau border is

$$A' = 2 \int_0^1 \frac{z'(1 - z') \left(\cos \theta_c - \frac{\text{Bo}}{2} z' \right)}{\left[1 - (1 - z')^2 \left(\cos \theta_c - \frac{\text{Bo}}{2} z' \right)^2 \right]^{1/2}} dz' \quad (\text{top PB}). \quad (16)$$

These results will be compared with experimental and simulated Plateau border shapes and areas in section V.

IV. NUMERICAL METHOD

We predict the shape of both the bottom and top Plateau borders numerically using Brakke's Surface Evolver [18]. We use cgs units throughout: the substrate separation in the

z direction is 2 cm (which is arbitrary provided the top and bottom Plateau borders do not touch), the value of gravity is taken to be 981 cm/s^2 , liquid density is 1 g/cm^3 ; then Plateau border areas are measured in cm^2 and surface tensions in mN (note that this is a 2D ‘line’ tension).

The simulation consists of just one half of the domain, by symmetry (see figure 5a), using just three fluid interfaces: one for the top Plateau border, one for the bottom Plateau border, and one for the vertical film joining them. All three have surface tension $\gamma = 28.2 \text{ mN}$, since the vertical film is one half of the physical double interface. To specify the contact angle θ_c at which the Plateau borders meet the substrates, we insert a further wetting film along the substrates, outside the Plateau borders, with tension $\gamma_{\text{wall}} = \gamma \cos \theta_c$.

Each Plateau border has fixed area and the two areas can be varied independently. We used a top Plateau border half-area of 0.005 cm^2 throughout, and increased the bottom Plateau border area to the required value (of up to about 0.3 cm^2) from an initial half-area of 0.020 cm^2 to explore different Bond numbers. Similarly, the contact angle θ_c is increased from zero in steps of one degree to allow all values up to 180° to be explored.

To allow the Plateau border surfaces to curve, each interface is discretised into N short straight segments; we expect a better representation of the interface at higher N , and illustrate the convergence to the analytic solution with increasing N in figure 8. The Surface Evolver is used to minimise the free energy of the system, i.e., the product of length and surface tension of the interfaces, subject to the fixed Plateau border areas. We evaluate the Hessian of energy frequently to ensure that the arrangement of films is a stable one [19].

The results of the simulation include Plateau border heights and widths, and the three interface lengths for different contact angles and Plateau border areas. They are compared with our theoretical predictions in the next section.

V. RESULTS AND DISCUSSION

In this section we compare theoretical, simulated and experimental results for Plateau border shapes. We first consider the shapes without gravity (V A). When gravity is included, that is at finite Bond number, we consider the bottom and top Plateau borders separately (V B and V C, respectively). For the bottom Plateau border, the experiments generate a variation in the Bond number by varying the size of the Plateau border, i.e., its liquid

content, although we note that this could also be achieved by changing the liquid density or its surface tension.

A. Film in zero gravity

First, it is instructive to consider the case $\text{Bo} = 0$, corresponding to zero gravity, for which the Plateau borders at the top and bottom substrates behave identically: their surfaces are arcs of circle. The integrals in equations (11) or (12), and (15) or (16) can now be performed analytically, yielding

$$x'(z') = \frac{1}{\cos \theta_c} \left\{ 1 - \left[1 - (1 - z')^2 \cos^2 \theta_c \right]^{1/2} \right\}, \quad (17)$$

$$A' = \frac{2}{\cos \theta_c} \left(1 - \frac{1}{2} \sin \theta_c - \frac{\frac{\pi}{2} - \theta_c}{2 \cos \theta_c} \right). \quad (18)$$

In particular, the half-width of the Plateau border at the substrate is

$$x'(z' = 0) = \frac{1 - \sin \theta_c}{\cos \theta_c}. \quad (19)$$

Figure 6 plots A' and $x'(z' = 0)$ given by equations (18) and (19), respectively. In the absence of gravity, the Plateau border can only exist if $\theta_c < \pi/2$, since its surfaces are circular arcs. In the limit $\theta_c \rightarrow 0$, we naturally have $x'(z' = 0) = 1$ and $A' \rightarrow 2 - \pi/2$, which corresponds to twice the difference between the areas of a square of side length 1 and of a quarter of a circle of unit radius inscribed in it. For $\theta_c \rightarrow \pi/2$, on the other hand, both $x'(z' = 0)$ and A' approach zero, because the film must extend vertically down (or up) to meet the substrate.

B. Film in non-zero gravity: bottom Plateau border

Figure 7 displays Plateau border shapes at the bottom substrate calculated using equation (11), for various combinations of Bo and θ_c . As might be intuitively expected, the Plateau border is widest at the substrate (i.e., at $z = 0$) for $\theta_c < 90^\circ$, but above the substrate (i.e., at some $z = z_{\max} > 0$) for $\theta_c > 90^\circ$. The height z_{\max} at which the Plateau border is widest can be found as a function of θ_c and Bo , but we do not present it here.

Figure 8 compares bottom Plateau border shapes from analytical theory and Surface Evolver simulations. Agreement is excellent at small contact angles, but less so at larger

contact angles and large Bond numbers where a very fine discretisation is needed to achieve sufficient accuracy in the simulations. This may be due to the considerable range of (concave and convex) curvatures of the bounding surfaces that exists in these cases, where discretisation errors may tend to accumulate more. In particular, for $\theta_c > 90^\circ$, for which $x'(z')$ has a maximum at z strictly greater than zero, the x location of this maximum is particularly sensitive to small errors in the inclination of the interface above it. In both cases, absolute errors are largest at the substrate ($z = 0$), because the film is pinned at $x = 0$ at the Plateau border apex. The other main difficulty in the simulations is that of approximating the zero degree contact angle at the Plateau border apex with *straight* segments; the inevitable small error here propagates along the surface, as described above.

Equations (11) and (15) do not yield physically meaningful results for all values of θ_c and Bo . We next discuss the non-trivial conditions defining their domains of validity.

For sufficiently strong gravity (i.e., sufficiently large Bo), the surfaces bounding the Plateau border may become horizontal at some point above the substrate, even if they are non-horizontal at the substrate, due to the fact that hydrostatic equilibrium favours higher pressure (and thus convex curvature) in the lowest parts of these surfaces. However, the inclination angle must not change sign, because $x'(z')$ would then become multiple-valued for a single z' . This is inconsistent with hydrostatic equilibrium, because it would imply a concave curvature existing at levels below a convex curvature (as illustrated schematically in figure 5c). The Plateau border surface may therefore only be horizontal at an inflection point, where $d^2x/dz^2 = 0$. This situation can be considered a threshold beyond which it becomes impossible to satisfy the Young-Laplace law, and thus beyond which the Plateau border is no longer physically realisable. It is therefore essential to determine this threshold. From equation (1) it can be seen that the film is horizontal when $\Delta p = 0$, corresponding to $dx/dz \rightarrow \infty$, or $\cos \theta = 1$, according to equation (9). This produces a singularity in the integral in equation (11) when the denominator of the integrand vanishes,

$$\frac{\text{Bo}}{2}z'^2 + \left(\cos \theta_c - \frac{\text{Bo}}{2}\right)z' + 1 - \cos \theta_c = 0, \quad (20)$$

which gives the vertical coordinates of the points where the film surface is horizontal (if they do exist). The solutions to equation (20) are

$$z' = \frac{\frac{\text{Bo}}{2} - \cos \theta_c \pm \sqrt{\left(\frac{\text{Bo}}{2} - \cos \theta_c\right)^2 - 2\text{Bo}(1 - \cos \theta_c)}}{\text{Bo}}. \quad (21)$$

When the expression under the square root is negative, no points exist at which the film is horizontal. The threshold where such points begin to exist occurs when this expression vanishes, namely when

$$\text{Bo}^2 + (4 \cos \theta_c - 8)\text{Bo} + 4 \cos^2 \theta_c = 0. \quad (22)$$

The solutions to this second-order algebraic equation for Bo are

$$\text{Bo} = 4 - 2 \cos \theta_c \pm \sqrt{(4 - 2 \cos \theta_c)^2 - 4 \cos^2 \theta_c}. \quad (23)$$

It is clear from equation (21) that the situation where two real solutions for z' exist, i.e., the domain of parameter space that is unphysical, corresponds to values of Bo outside the interval bounded by the solutions given by equation (23). It can be shown, however, that in the lower range of values outside this interval, $\cos \theta = 1$ is not fulfilled for $0 < z' < 1$, so only the inequality involving the largest root (with the plus sign in equation (23)) is relevant; the model then becomes unphysical when

$$\text{Bo} > 4 - 2 \cos \theta_c + \sqrt{(4 - 2 \cos \theta_c)^2 - 4 \cos^2 \theta_c}. \quad (24)$$

For each value of θ_c , the right-hand side of equation (24) defines an upper bound for Bo, or equivalently an upper bound for h , for which the bottom Plateau border is physically realisable and the surface foam-philic.

Another condition for the validity of equations (11) and (15) follows from requiring that the Plateau border is topologically sound. Equation (11) specifies the horizontal coordinate of the right-hand surface at the substrate, $x'(z' = 0)$. In the most usual situations, the contact angle θ_c lies between 0 and $\pi/2$ (hydrophilic surface), which implies that $x'(z')$ given by equation (11) is always positive, as $z' < 1$ by definition. When the substrate is hydrophobic ($\pi/2 < \theta_c < \pi$), however, the numerator of the fraction in the integrand of equation (11) may become negative, and therefore $x'(z)$ may also be negative. This, which is easiest to fulfil for $x'(z' = 0)$ (as the term involving Bo in the numerator is always non-negative), is unphysical, since $x'(z' = 0) < 0$ would correspond to Plateau border surfaces that cross each other before reaching the substrate (see figure 5b).

Equations (11) and (15) are therefore only valid outside the interval defined by equation (24) and when $x'(z' = 0) \geq 0$. the Plateau border area A' given by equation (15) may also be negative for hydrophobic substrates ($\theta_c > \pi/2$), but the domain of parameter space where

$A' < 0$ is contained in the (equally unphysical) domain where $x'(z' = 0) < 0$, because one may have $x'(z' = 0) < 0$, but $x'(z' > 0) > 0$. That is, the (negative) area below the point where the Plateau border surfaces cross may not fully compensate for the (positive) area above that point. Although the domains defined by $x'(z' = 0) < 0$ or $A' < 0$ are unphysical, one can still solve the Young-Laplace equation and find $x'(z')$ and A' in such cases. Note that, on the contrary, this is not possible in the forbidden domain defined by equation (24), because in that case the Young-Laplace equation breaks down.

The above findings are summarised in figure 9a. The cross-hatched domain is where inequality (24) is satisfied and hence where there can be no Plateau border because no solution to the Young-Laplace equation exists. The shaded domain is where $x'(z' = 0) < 0$, i.e., the left and right Plateau border surfaces intersect before meeting the substrate or switch places altogether. Examples of Plateau border shapes in this domain are given in figure 10 (top row). Both cross-hatched and shaded domains thus consist of (θ_c, Bo) pairs for which no bottom Plateau border can exist – ‘forbidden’ states – separated by a white band of ‘allowed’ states. Furthermore, allowed Plateau borders may exhibit an inflection point, at which the curvature of their liquid-vapour interfaces changes from convex near the substrate to concave near the apex. Since inflection points correspond to $\Delta p = 0$, they will first appear when this condition is fulfilled at the substrate, $z = 0$. From equation (6) and using the definition of Bo, we obtain the threshold

$$\text{Bo} = 2 \cos \theta_c, \quad (25)$$

which is plotted as the dashed line in figure 9a. Below this line, Plateau borders do not have inflection points; above it they do, owing to the effect of gravity. The z coordinate of the inflection point can also be found from the theory, but this is beyond the scope of the present study. Clearly, most realisable Plateau borders do have inflection points, i.e., the curvature of their surfaces changes sign, from convex near the substrate to concave nearer the apex.

The solid curves inside the white (allowed) and shaded (forbidden) parameter domains are lines of constant $x'(z' = 0)$ as labelled. At constant θ_c , $x'(z' = 0)$ increases as Bo is increased, which seems an intuitive effect of gravity. The same qualitative trend occurs for A' (not shown). In the white domain $x'(z' = 0)$ varies from 0 at the lower boundary to a value that is a function of θ_c , but always greater than 1, at the upper boundary. This

latter limit corresponds to a situation where the Plateau border is strongly ‘flattened’ by gravity. We could not determine any bound for $x'(z' = 0)$ (or for the corresponding area A') as Bo approaches this limit. This means that both quantities can potentially become very large, although the range of Bo in which this occurs is very narrow, and therefore should be difficult to access in practice.

Figure 11 shows photographs of Plateau borders (equivalent of side view in figure 2b) at the liquid film-surface interface for four of the five surfaces used in the experiments, overlaid with their analytically-calculated shapes for the same Bond numbers and contact angles. Then figure 12 compares theoretical predictions and experimental results for the Plateau border half-width x , scaled by its height h , *vs* Bond number. (Equation (11) has been used in both cases.) The general trends of x/h are well reproduced, with the only substantial deviation occurring for the most hydrophobic substrate (teflonised black silicon) at $Bo \approx 8$. Since the vertical asymptotes of the theoretical curves correspond to the upper Bo limit mentioned in the preceding paragraph, it is to be expected that experimental results in these regions should be more sensitive to, for example, errors in measuring h , from which Bo is calculated. This might explain the poorer agreement between theory and experiment in the upper Bo range of each curve. One other possible source of discrepancy is contact angle hysteresis, which is neglected in our theory and simulations but should be more pronounced at large Bo .

C. Film in non-zero gravity: top Plateau border

A similar analysis can be performed to determine the validity of equations (12) and (16) for the top Plateau border. Note that now the z' -axis is directed downwards from $z' = 0$ (the top substrate). Since, because of hydrostatic equilibrium, their curvature must become less convex, or more concave, as z' decreases, the only way that the surfaces can become horizontal at an inflection point before reaching the substrate (which defines a threshold for the existence of solutions to the Young-Laplace equation) is by having convex curvature at the bottom. This requires that the film surfaces cross (unphysically) immediately at the apex where the Plateau border meets the planar film underneath. The condition to be fulfilled for the existence of a solution to the Plateau border surfaces is then $\cos \theta = -1$,

which corresponds to a singularity in the integrand of equation (12) if

$$\frac{\text{Bo}}{2}z'^2 - \left(\cos\theta_c + \frac{\text{Bo}}{2}\right)z' + 1 + \cos\theta_c = 0, \quad (26)$$

yielding

$$z' = \frac{\frac{\text{Bo}}{2} + \cos\theta_c \pm \sqrt{\left(\frac{\text{Bo}}{2} + \cos\theta_c\right)^2 - 2\text{Bo}(1 + \cos\theta_c)}}{\text{Bo}}. \quad (27)$$

Now, the condition for the threshold at which $x'(z')$ becomes multivalued is

$$\text{Bo}^2 - (4\cos\theta_c + 8)\text{Bo} + 4\cos^2\theta_c = 0, \quad (28)$$

the solution of which is

$$\text{Bo} = 4 + 2\cos\theta_c \pm \sqrt{(4 + 2\cos\theta_c)^2 - 4\cos^2\theta_c}. \quad (29)$$

A similar argument as used previously applies to the two roots of equation (29), so that we take the largest root to allow us to predict the ‘forbidden’ domain of parameter space where the Young-Laplace equation has no solution:

$$\text{Bo} > 4 + 2\cos\theta_c + \sqrt{(4 + 2\cos\theta_c)^2 - 4\cos^2\theta_c}. \quad (30)$$

This equation is equivalent to equation (24) if the sign of $\cos\theta_c$ is reversed.

Note that, as with the bottom Plateau border, in the domain of parameter space where inequality (30) is not satisfied there are many (θ_c, Bo) pairs for which the Young-Laplace equation has a solution, but $x'(z' = 0) < 0$ and $A' < 0$, which is obviously unphysical on topological grounds. However, neither of these criteria may now be used to delimit the allowed domains of parameter space, as there are solutions with $x'(z' = 0) > 0$ or $A' > 0$ for which the two Plateau border surfaces still cross. Since, from hydrostatic equilibrium, the most convex curvature of the Plateau border surfaces must exist near their lowest point, this is where they are most likely to cross. The only way to avoid this topological violation is by requiring that the curvature should not be convex at the point where the Plateau border surfaces meet the planar film below. Hence, the threshold condition for the realisability of the Plateau border is, in this case, having zero curvature at the lower end of the surfaces bounding the Plateau border, i.e., $d^2x/dz^2(z = h) = 0$, thereby avoiding convex curvature altogether. This condition, again, corresponds to $\Delta p = 0$. Given the definition of Δp for the top Plateau border, namely

$$\Delta p = p_{b0} - p_a + \rho g z, \quad (31)$$

and the modified form of equation (6) that results,

$$\frac{p_a - p_{b0}}{\gamma} = \frac{1}{h} \cos \theta_c + \frac{\rho g h}{2\gamma}, \quad (32)$$

equation (31) can be inserted into equation (32) for $z = h$ and $\Delta p = 0$ to yield

$$\text{Bo} = 2 \cos \theta_c. \quad (33)$$

Interestingly, this is exactly the same as the threshold for a bottom Plateau border to have an inflection point, equation (25). The difference here is that, since (by the above arguments) a top Plateau border cannot have any inflection points, equation (33) now assumes the much more important role of defining an upper bound for Bo beyond which no top Plateau border can exist.

The above findings are summarised in figure 9b. As in figure 9a, the white domain comprises (θ_c, Bo) pairs for which the Plateau border half-width at the (in this case top) substrate is positive; as explained above, this is a necessary (but not sufficient) condition for the Plateau border to be physically realisable. In the shaded domain, by contrast, $x'(z' = 0) < 0$.

Although, as for the bottom Plateau border, equation (12) can still be solved in the shaded domain of figure 9b, the resulting Plateau borders are unphysical. In the cross-hatched domain, which is a mirror image of that found for the bottom Plateau border, the Young-Laplace equation has no solution. However, in contrast to figure 9a, the white region in figure 9b does not now coincide with the domain where the Plateau border is realisable: this is only so in the much smaller domain below the dashed line, which is given by equation (33). In other words, at the top substrate only Plateau borders with no inflection points can exist – their surfaces are always concave. Examples of unphysical top Plateau border shapes are provided in figure 10 (bottom row). Note also that both $x'(z' = 0)$ (shown in figure 9b) and A' (not shown) decrease as Bo is increased at constant θ_c , which again is expected given the direction of gravity.

As might be intuitively expected, Plateau borders can only exist at the top substrate if the liquid contact angle $\theta_c \leq \pi/2$, otherwise the liquid will just detach from the substrate. Values of $x'(z' = 0)$ in the white domain below the dashed line in figure 9b are all below 1, which illustrates how gravity acts to stretch the top Plateau border vertically (and consequently compress it horizontally), especially for the largest allowed values of Bo, as can be seen in

figure 13 (calculated using equations (11) and (12) for the bottom and top Plateau borders, respectively).

A relevant question that may be asked is: how large, in physical dimensions, can the Plateau borders be? Given our comments above, about x' and A' being unbounded as Bo approaches its upper limit, the bottom Plateau border can probably be indefinitely large, expanding laterally as more fluid is added to it. On the other hand, the answer for the top Plateau border is totally different. First, as noted above, no top Plateau border can exist on a hydrophobic substrate ($\theta_c > 90^\circ$), since it would detach due to gravity. When the substrate is hydrophilic ($\theta_c < 90^\circ$), however, there is an upper bound to the size of the top Plateau border, which depends on the contact angle, and naturally approaches zero as $\theta_c \rightarrow 90^\circ$. The area of the top Plateau border given by equation (16) is normalised by h^2 , so it does not give us information about the physical size of the Plateau border. A more useful quantity is obtained by multiplying A' by Bo , which gives $\rho g A / \gamma \equiv A / \lambda_c^2$, i.e., the Plateau border area normalised by the square of the capillary length $\lambda_c = (\gamma / \rho g)^{1/2}$. Whereas for Bo in the range $(0, 2 \cos \theta_c)$ A' attains maximum values for $\text{Bo} = 0$ (and an absolute maximum for $\theta_c = 0$), $\rho g A / \gamma$ attains its maximum values for $\text{Bo} = 2 \cos \theta_c$. Figure 14 shows how the maximum of A / λ_c^2 (calculated using equation (16) for $\text{Bo} = 2 \cos \theta_c$) varies as a function of θ_c . It can be seen that A / λ_c^2 attains an absolute maximum of 0.396 for $\theta_c = 0$. Not surprisingly, this indicates that this maximum of A is of the order of the capillary length squared. Using the experimental values $g = 9.81 \text{ ms}^{-2}$ and $\gamma = 28 \text{ mN/m}$ yields an absolute maximum for A of 1.138 mm^2 .

VI. CONCLUSIONS

We have studied the shapes of the Plateau borders at which a vertical planar liquid film meets horizontal substrates of various wettabilities, by analytical theory, numerical simulation, and experiment. The overall picture that emerges is that the Plateau borders, and consequently the film to which they are attached, spanning the gap between the two substrates, can only be realised in certain ranges of Plateau border sizes, which are in turn functions of the liquid contact angle. In other words, a foam-surface system can be either ‘foam-phobic’ or ‘foam-philic’. The Plateau border at the top substrate has quite a small domain of existence and a necessary condition is that the liquid contact angle is less than

90°. Its maximum area decreases as the contact angle increases, and attains an absolute maximum of 0.396 times the square of the capillary length, for $\theta_c = 0$. The Plateau border at the bottom substrate has a larger domain of existence, larger contact angles being required at higher Bond numbers and vice versa. The practical importance of this is that both surface and liquid (foam) properties need to be taken into account in applications where wetting of surfaces by foams plays a role. It suggests, e.g., that self-cleaning surfaces for foams could be designed and built.

We are currently working on generalising our results to a bubble on a solid substrate. We expect qualitatively the same results, although the detailed shapes of the ‘allowed’ and ‘forbidden’ domains in (θ_c, Bo) parameter space will likely be different.

Acknowledgements

The work of S. A. was partly supported by the French RENATECH network. S. J. C. thanks K. Brakke for his development and maintenance of the Surface Evolver code and acknowledges funding from the MSCA-RISE project Matrixassay (ID: 644175). P. I. C. T. acknowledges financial support from the Fundação para a Ciência e Tecnologia (Portugal) through contracts nos. EXCL/FIS-NAN/0083/2012 and UID/FIS/00618/2013. S. A. would very much like to thank Thomas Arscott for fruitful discussions concerning the experimental setup. We are grateful to W. Drenckhan for a critical reading of the manuscript.

-
- [1] Rowlinson, J. R.; Widom, B. *Molecular Theory of Capillarity*; Oxford, Clarendon Press, 1982.
 - [2] Gao, L.; McCarthy, T. J.; Zhang, X. Wetting and superhydrophobicity. *Langmuir* **2009**, *25*, 14100–14104.
 - [3] Gao, L.; McCarthy, T. J. Wetting 101. *Langmuir* **2009**, *25*, 14105–14115.
 - [4] Shirtcliffe, N. J.; McHale, G.; Atherton, S.; Newton, M. I. An introduction to superhydrophobicity. *Adv. Coll. Interf. Sci.* **2009**, *161*, 124–138.
 - [5] Fortes, M. A.; Teixeira, P. I. C. Excess energy of a Plateau border at a wall. *Phil. Mag. Lett.* **2005**, *85*, 21–25.
 - [6] Teixeira, P. I. C.; Fortes, M. A. Line tension and excess energy of a wall Plateau border. *Phys.*

Rev. E, **75**, 011404.

- [7] Teixeira, M. A. C.; Teixeira, P. I. C. Contact Angle of a Hemispherical Bubble: An Analytical Approach. *J. Colloid Interface Sci.* **2009**, *338*, 193–200.
- [8] Teixeira, M. A. C.; Arscott, S.; Cox, S. J.; Teixeira, P. I. C. What is the shape of an air bubble on a liquid surface? *Langmuir* **2015**, *31*, 13708–13717.
- [9] Cantat, I.; Cohen-Addad, S.; Elias, F.; Graner, F.; Höhler, R.; Pitois, O.; Rouyer, F.; Saint-Jalmes, A. *Foams: Structure and Dynamics*; Oxford University Press, 2013.
- [10] Cantat, I. Liquid meniscus friction on a wet plate: Bubbles, lamellae, and foams. *Phys. Fluids* **2013** *25*, 031303.
- [11] Arscott, S. Wetting of soap bubbles on hydrophilic, hydrophobic, and superhydrophobic surfaces, *Appl. Phys. Lett.* **2015**, *102*, 254103–4.
- [12] Arscott, S. Dynamic Chemically Driven Dewetting, Spreading, and Self-Running of Sessile Droplets on Crystalline Silicon. *Langmuir* **2016**, *32*, 12611–12622.
- [13] Zhuang, Y. X.; Menon, A. Wettability and thermal stability of fluorocarbon films deposited by deep reactive ion etching. *J. Vac. Sci. Technol. A* **2005**, *23*, 434–439.
- [14] Stubenrauch, M.; Fischer, M.; Kremin, C.; Stoebenau, S.; Albrecht, A.; Nagel, O. Black silicon – new functionalities in microsystems, *J. Micromech. Microeng.* **2006**, *16*, S82–S87.
- [15] Brinkmann, M.; Blossey, R.; Arscott, S.; Druon, C.; Tabourier, P.; Le Gac, S.; Rolando, C. Microfluidic design rules for capillary slot-based electrospray sources, *Appl. Phys. Lett.* **2004**, *85*, 2140–2142.
- [16] Drenckhan, W.; Dollet, B.; Hutzler, S.; Elias, F. Soap films under large-amplitude oscillations. *Phil. Mag. Lett.* **2008**, *88*, 669–677.
- [17] Isenberg, C. *The Science of Soap Films and Soap Bubbles*; Courier Corporation, 1978.
- [18] Brakke, K. The Surface Evolver. *Exp. Math.* **1992**, *1* (2), 141–165 (see also <http://facstaff.susqu.edu/brakke/evolver/evolver.html>).
- [19] Brakke, K. The Surface Evolver and the stability of liquid surfaces. *Trans. R. Soc. A* **1996**, *354*, 2143–2157.

	Material	Contact angle to bubble solution (deg)
Surface 1	Silicon oxide	18.2 ± 2.8
Surface 2	Teflonised polished silicon	51.7 ± 0.3
Surface 3	PDMS elastomer	61.0 ± 2.1
Surface 4	Teflonised rough silicon	64.0 ± 0.4
Surface 5	Teflonised black silicon	109.3 ± 0.3

TABLE I: List of surfaces prepared and used in this study and their measured wetting contact angle with the commercial bubble solution.

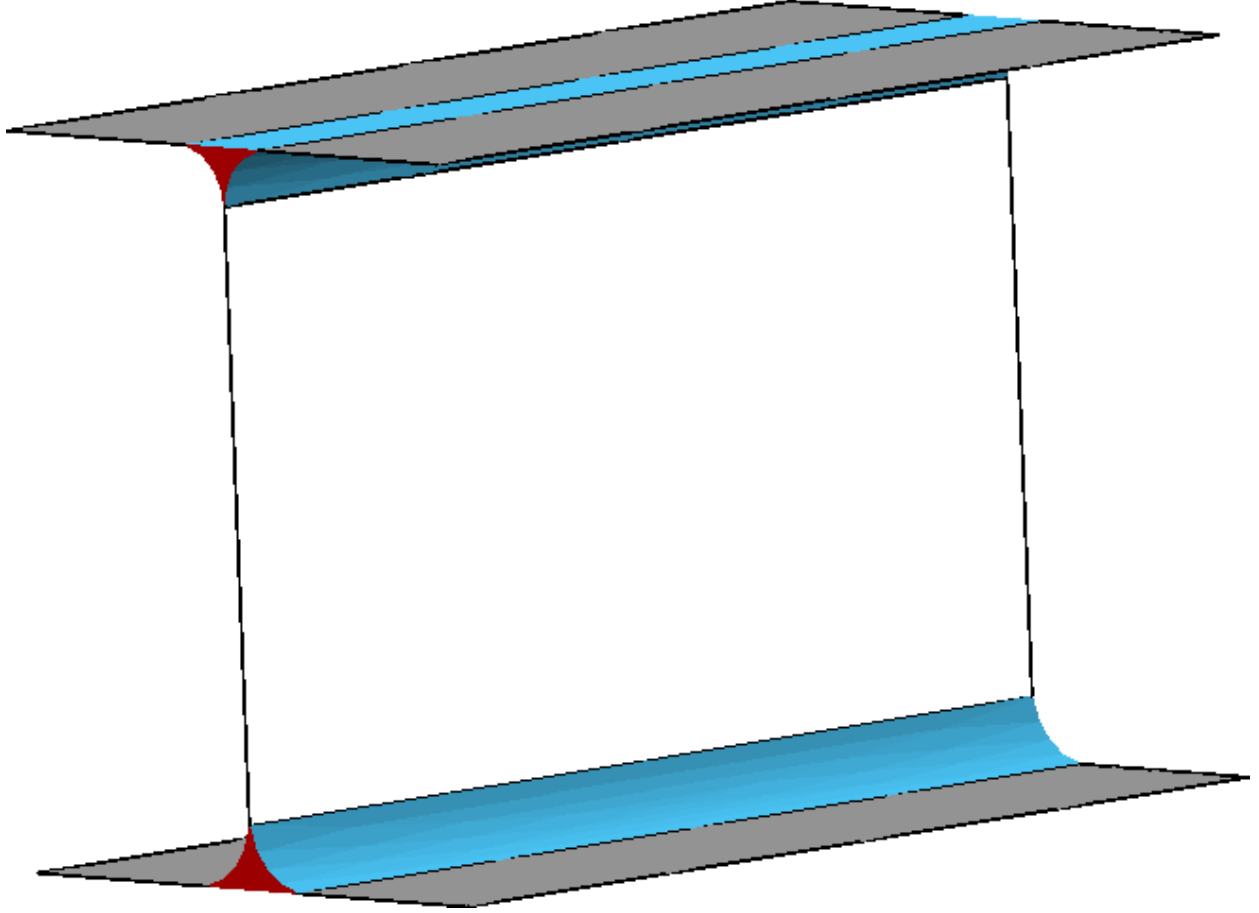


FIG. 1: Surface-Evolver-generated oblique view of a soap film spanning the gap between two parallel walls. The film (transparent) meets the walls (grey) at surface Plateau borders (blue). Each surface Plateau border is bounded by the solid wall and by two curved liquid-vapour interfaces. If the film is planar then the Plateau borders have uniform cross-section (red) along a direction parallel to both the film and the walls, and is thus effectively 2D.

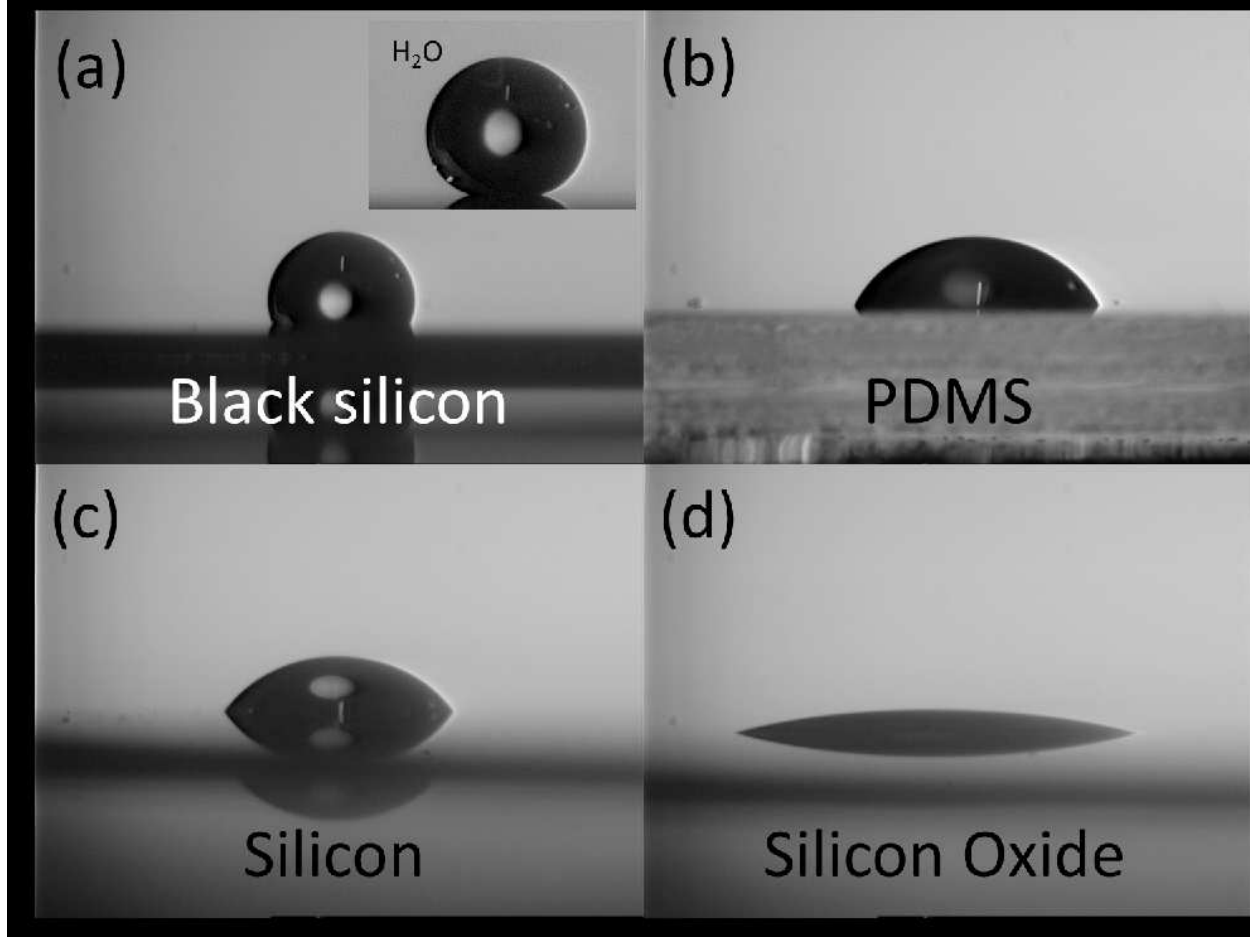


FIG. 2: Droplets of the bubble solution on four of the five different surfaces used in the experimental part of the study: (a) teflonised black silicon; (b) PDMS elastomer; (c) teflonised polished silicon; and (d) silicon oxide. The inset to panel (a) shows a water droplet resting on a teflonised black silicon surface. The droplet base diameters in (a) to (d) are 1.9 mm, 3.4 mm, 3.2 mm and 5.6 mm. The diameter of the droplet in the inset to (a) is 2.6 mm.

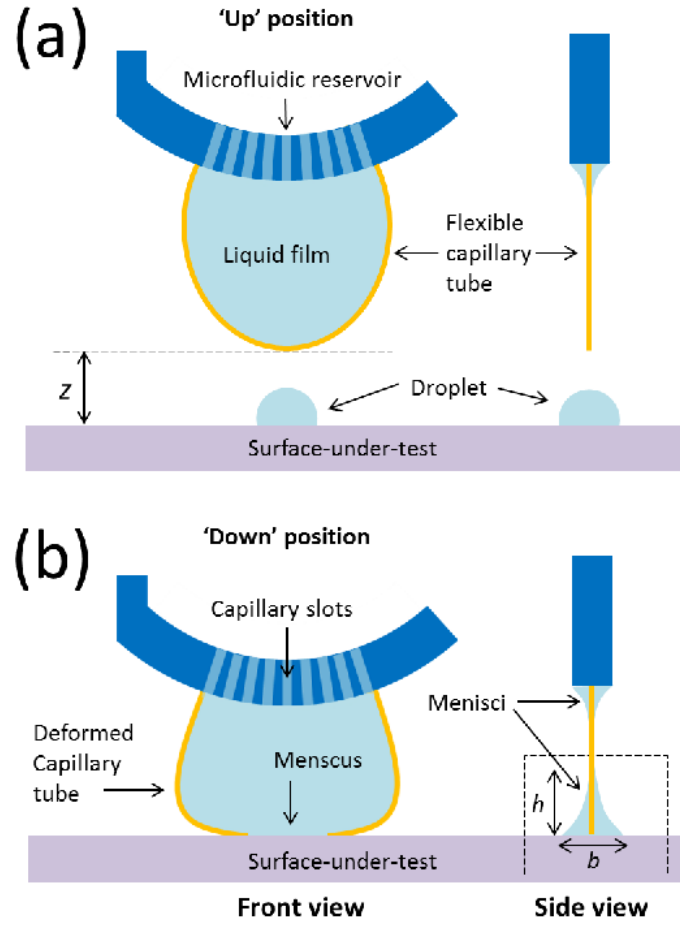


FIG. 3: Schematic diagram showing the experimental setup – front view and side view. The in-house microfluidic tool is in (a) the ‘up position’, and (b) the ‘down position’. The tool consists of a microfluidic reservoir (dark blue) and a deformable loop (gold) holding the liquid film (light blue). The tool is placed inside the contact angle meter. The dashed box indicates the photograph shown in figure 11.

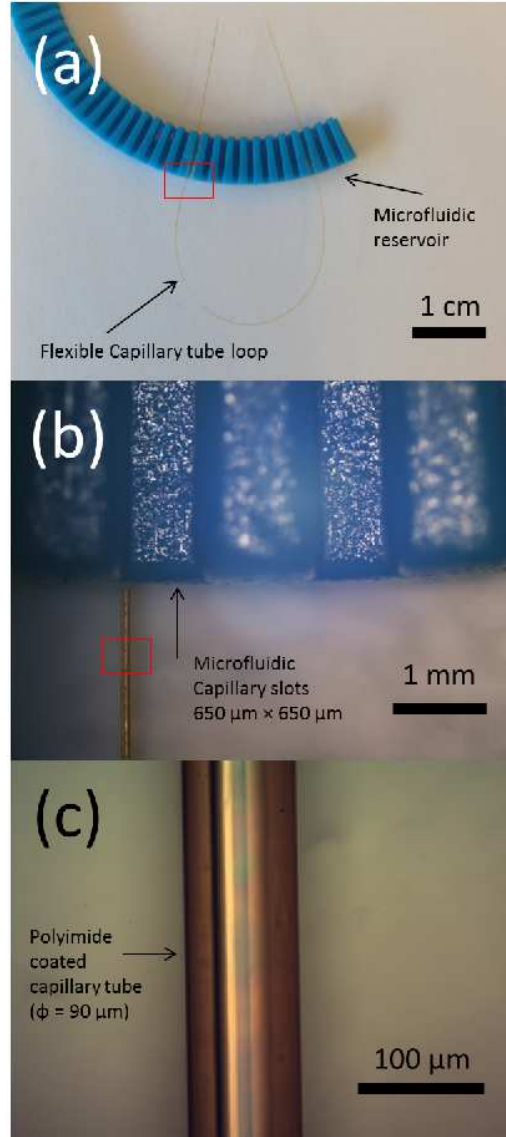


FIG. 4: Photographs of the parts of the microfluidic tool. (a) The microfluidic reservoir (blue) containing the capillary slots and the capillary tube which forms a deformable loop; (b) Zoom of the microfluidic capillary slots made of plastic (ABS); and (c) zoom of the flexible polyimide-coated, fused silica capillary tube (outside diameter 90 μm). The red boxes indicate the zoom regions.

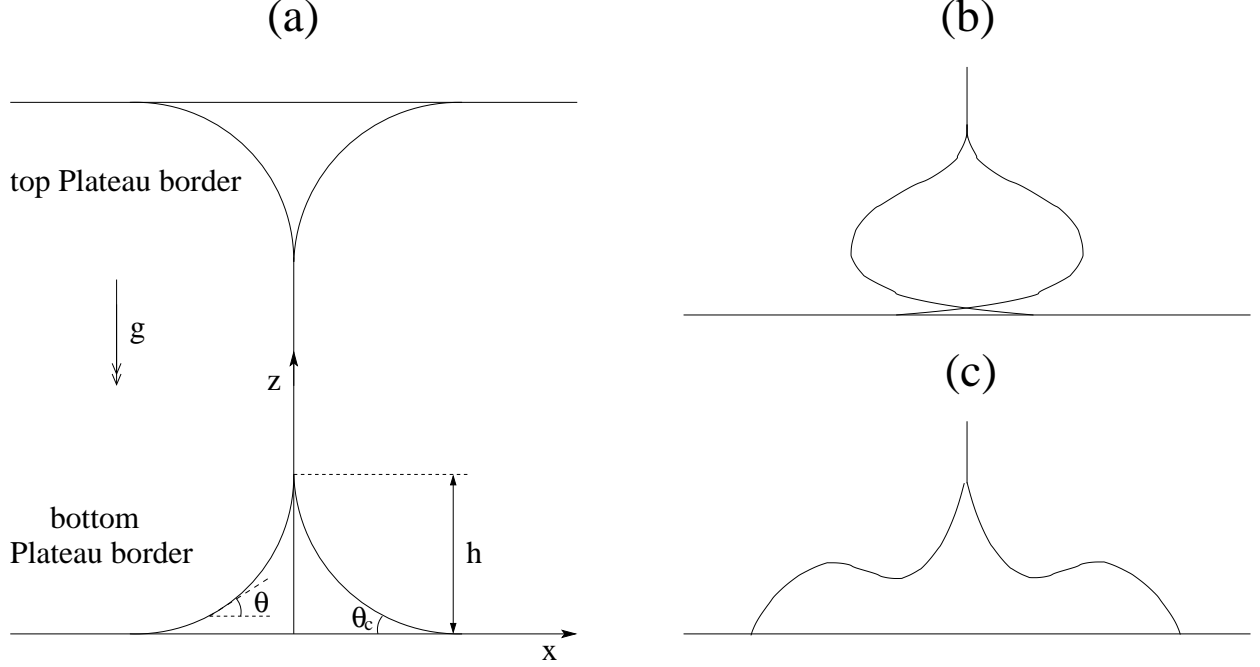


FIG. 5: (a) Sketch of a slab-symmetric soap film spanning the gap between two flat horizontal substrates and the associated surface Plateau borders: z is the height, x is the distance from the film (the z -axis) to the Plateau border surface, h is the Plateau border height, θ is the Plateau border inclination, and θ_c is the liquid contact angle at the substrate, located at $z = 0$. The gravitational acceleration is g . (b) Sketch of an unphysical surface Plateau border in the lower forbidden domain of figure 9a. (c) Sketch of an unphysical surface Plateau border in the upper forbidden domain of figure 9a.

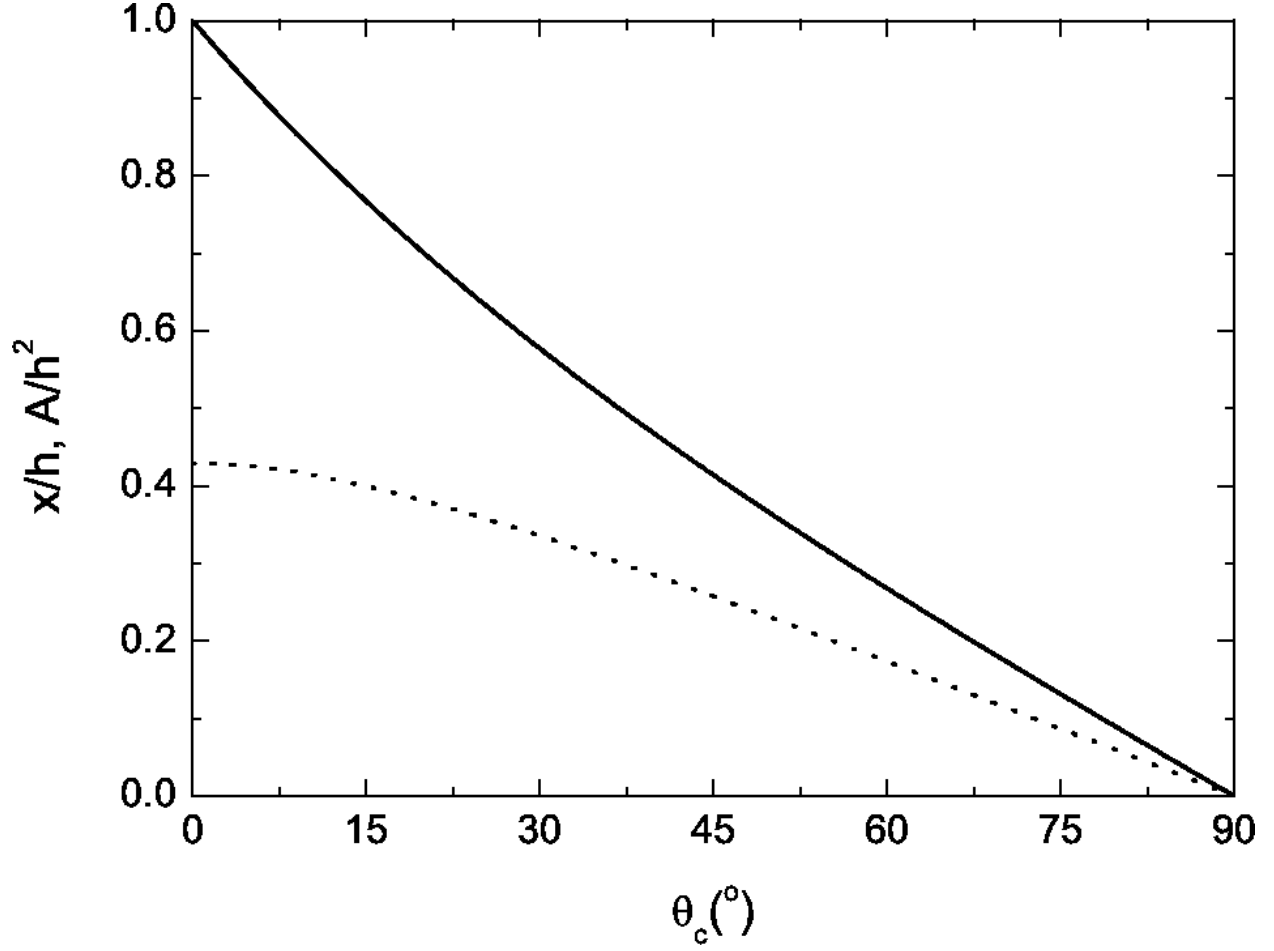


FIG. 6: Dimensionless Plateau border half-width at the substrate $x'(z' = 0)$ (solid line) and dimensionless Plateau border area A' (dotted line) *vs* contact angle θ_c for $\text{Bo} = 0$ (corresponding to zero gravity). Recall that in this case the top and bottom Plateau borders are identical.

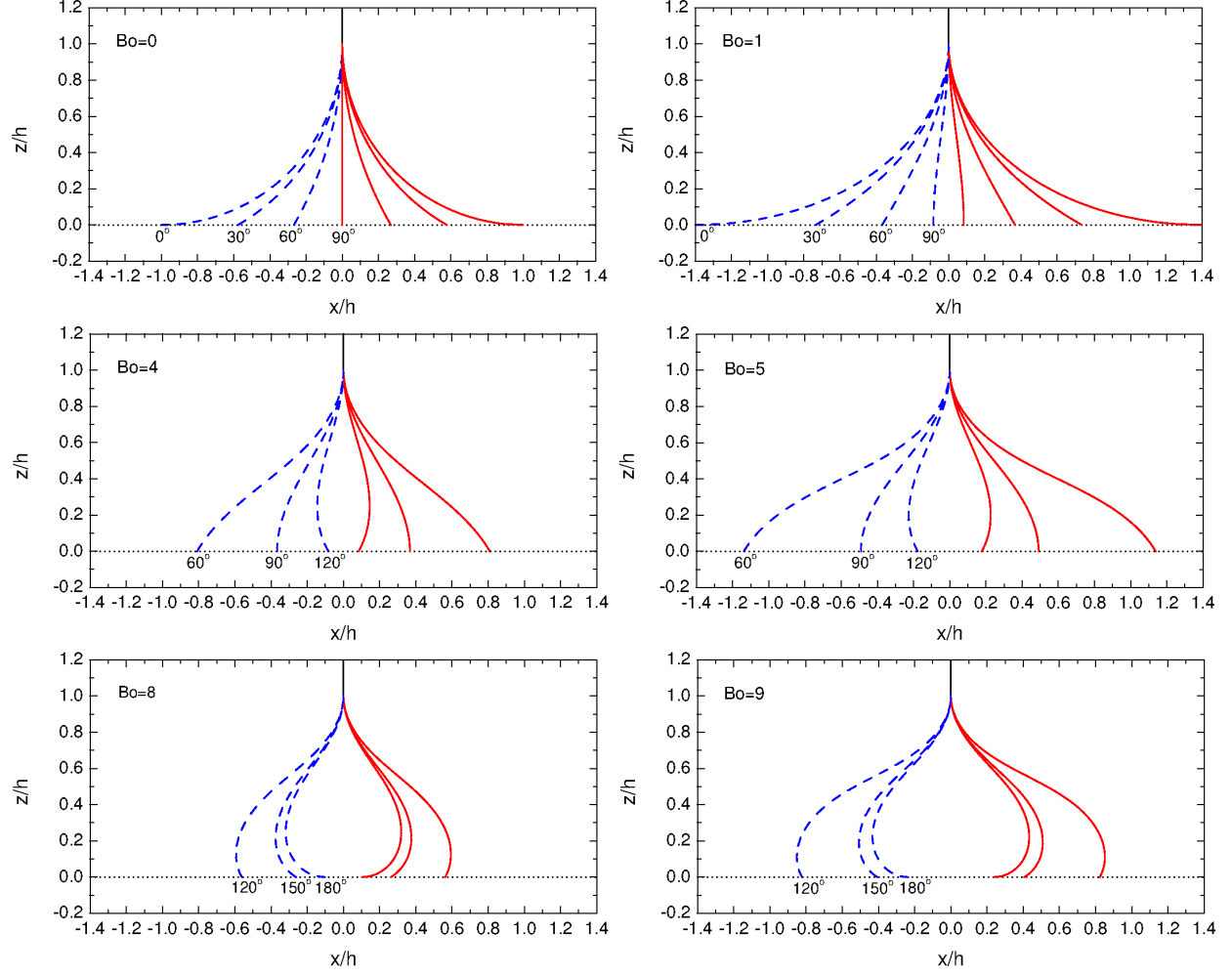


FIG. 7: Analytically-calculated Plateau border shapes at the bottom substrate, for Bo and θ_c as given. The left-hand air-liquid interfaces are shown as dashed blue lines, the right-hand ones as solid red lines.

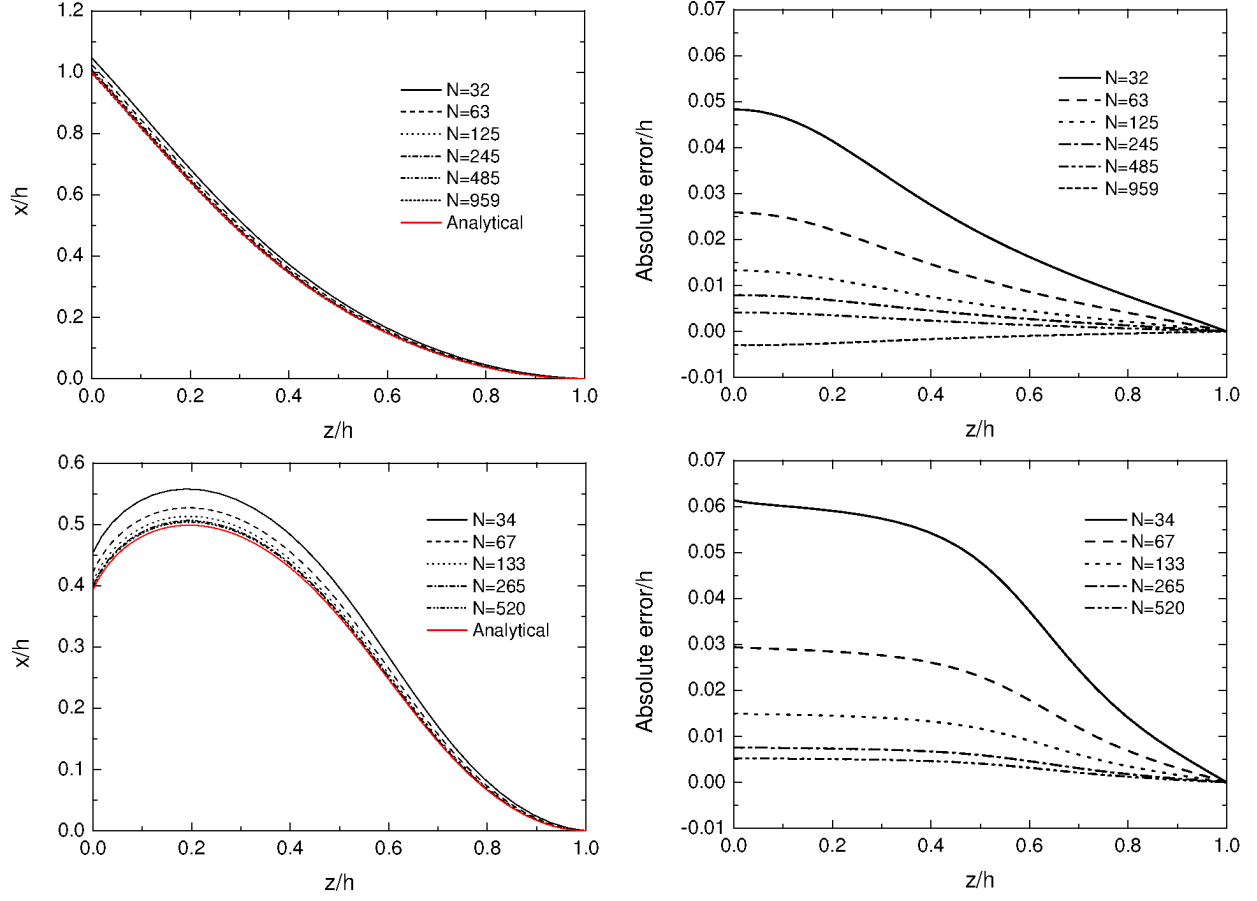


FIG. 8: Left column: Plateau border shapes from analytical theory (red lines) and from Surface Evolver with various levels of refinement, as given by the number of line segments N used to discretise the interface (black lines). Right column: absolute errors at each height z , defined as the difference between each of the Surface Evolver curves and the analytical theory curve in the left panel of the same row. Top row: $Bo = 2.138457$, $\theta_c = 30^\circ$. Bottom row: $Bo = 8.975624$, $\theta_c = 151^\circ$.

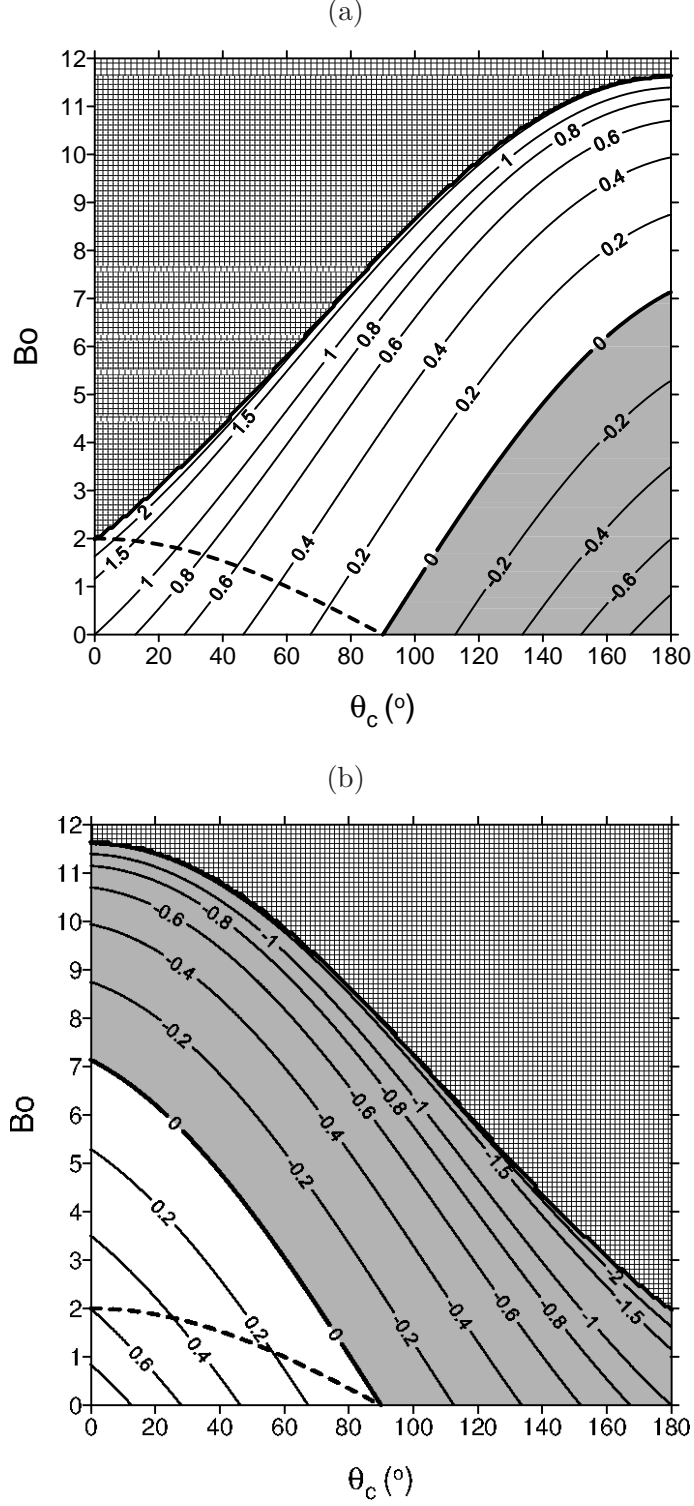


FIG. 9: Domains of allowed and forbidden Plateau borders at (a) the bottom substrate, and (b) the top substrate, in the space of liquid contact angle θ_c and Bond number Bo . The curves are lines of constant $x'(z' = 0)$ as labelled. See the text for details.

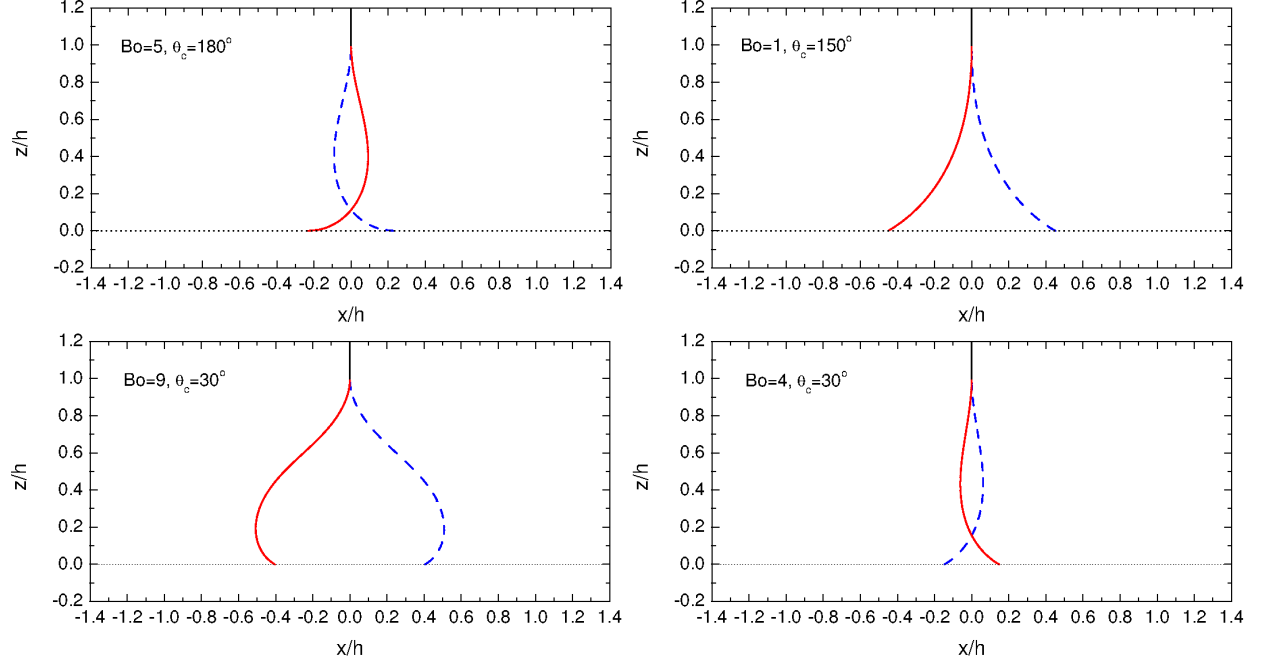


FIG. 10: Examples of unphysical Plateau borders in the shaded domain of figure 9a (top row); the shaded domain of figure 9b (bottom left); and the white domain of figure 9b, above the dashed line (bottom right)

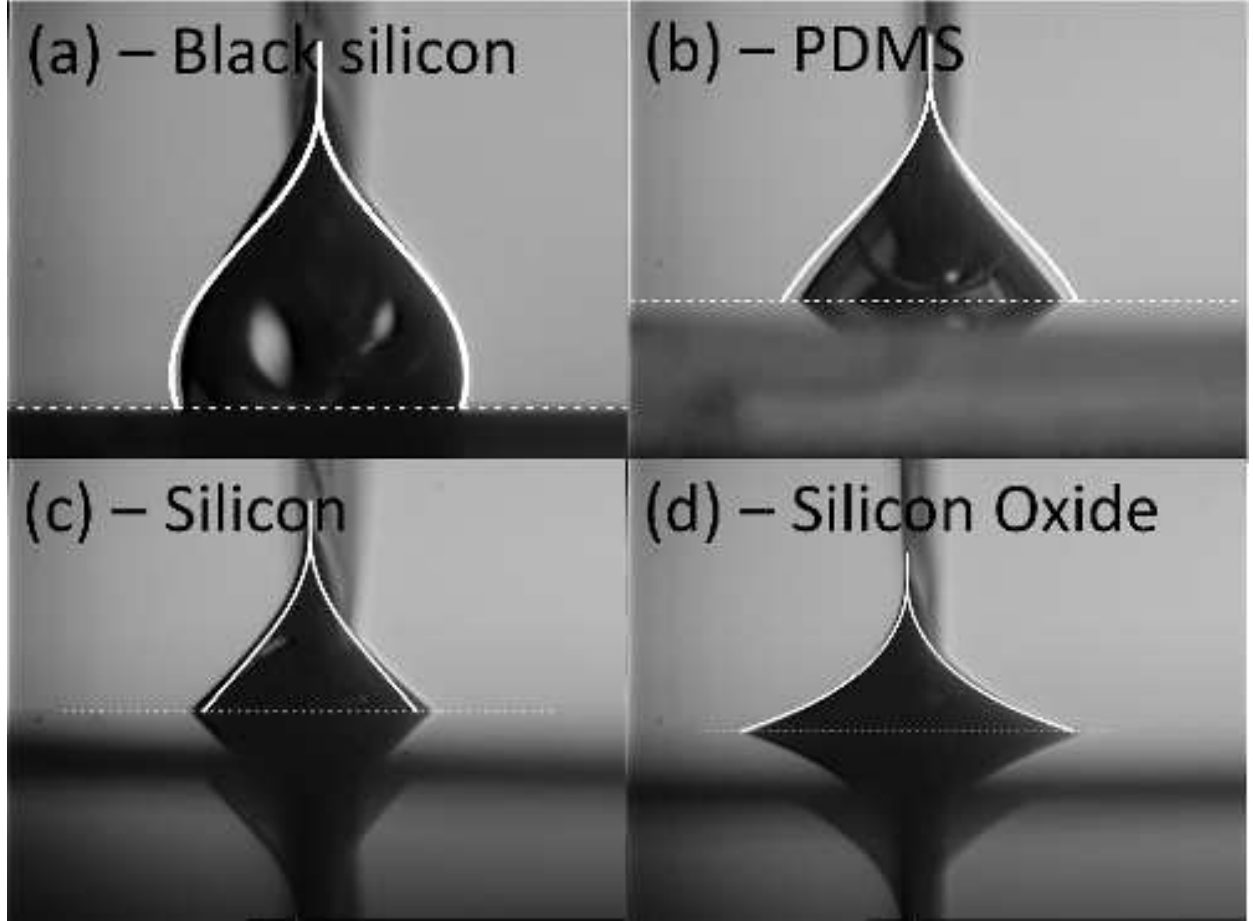


FIG. 11: Plateau borders at the liquid film-surface interface for four of the five substrates used in the experiments. (a) Teflonised black silicon; (b) PDMS elastomer; (c) teflonised polished silicon; and (d) silicon oxide. The Bond numbers and Plateau border base widths are: (a) $Bo = 6.65$ and 3.8 mm; (b) $Bo = 3.36$ and 3.7 mm; (c) $Bo = 2.13$ and 3.4 mm; and (d) $Bo = 1.59$ and 4.7 mm. The solid white lines are the analytically-calculated Plateau border shapes for the same Bond number and contact angle.

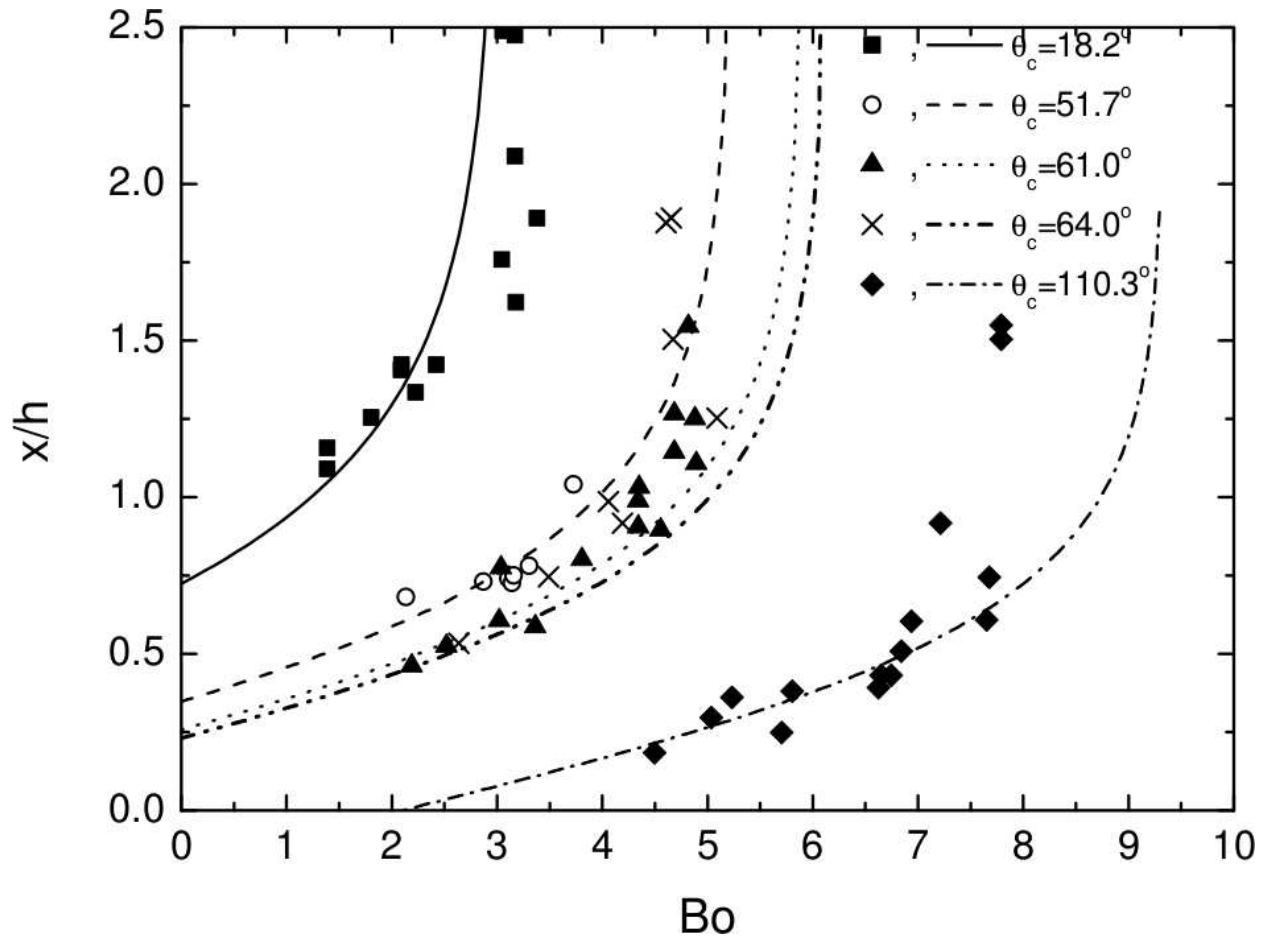


FIG. 12: Scaled Plateau border half-width x/h vs Bond number, for all five substrates investigated. The curves are theoretical predictions, symbols are experimental data points.

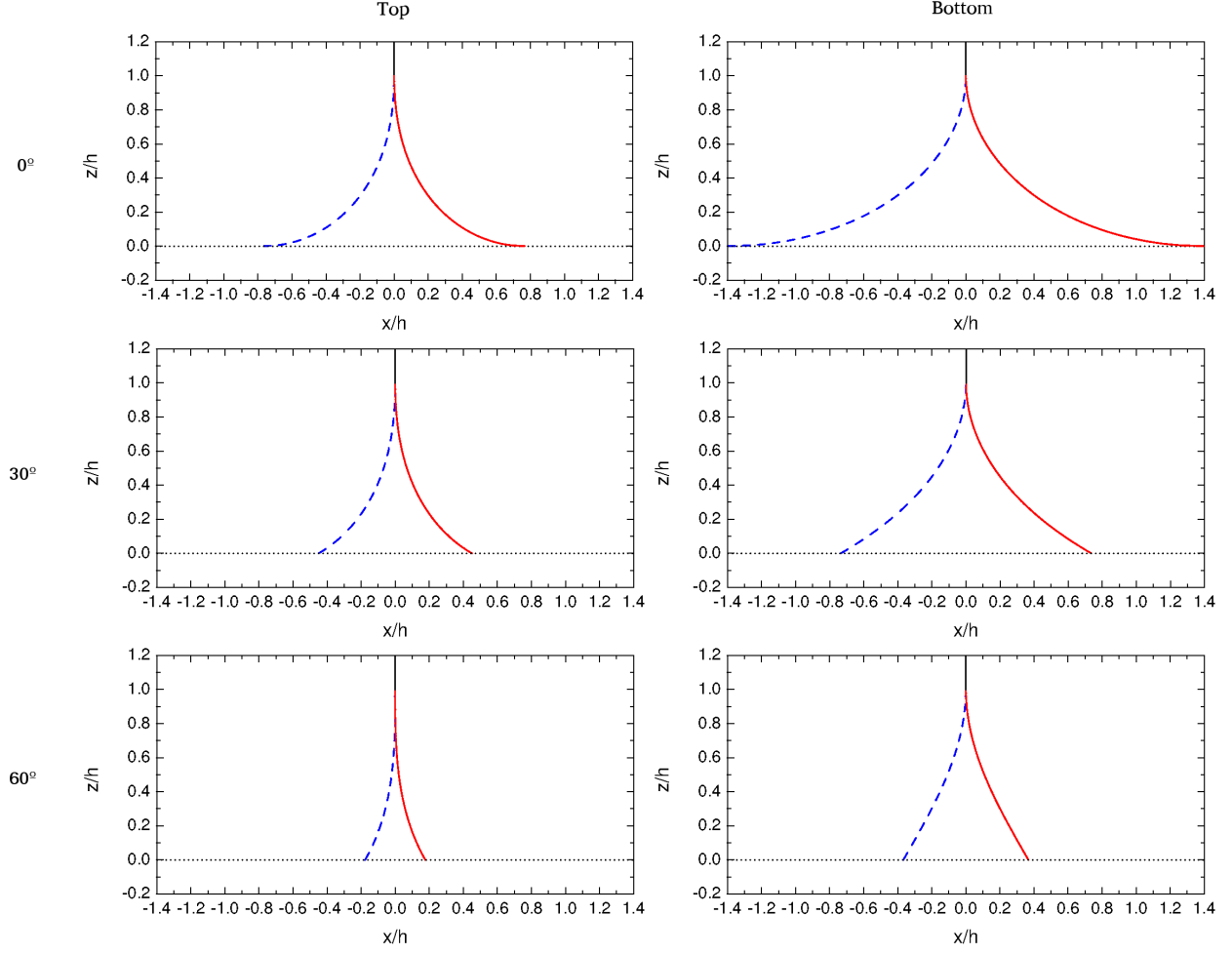


FIG. 13: Analytically-calculated Plateau border shapes at the top (left column) and bottom (right column) substrates, for $Bo = 1$ and $\theta_c = 0^\circ$ (top row), 30° (centre row) and 60° (bottom row). The left-hand air-liquid interfaces are shown as dashed blue lines, the right-hand ones as solid red lines. The Plateau borders at the top substrate are shown inverted for ease of comparison.

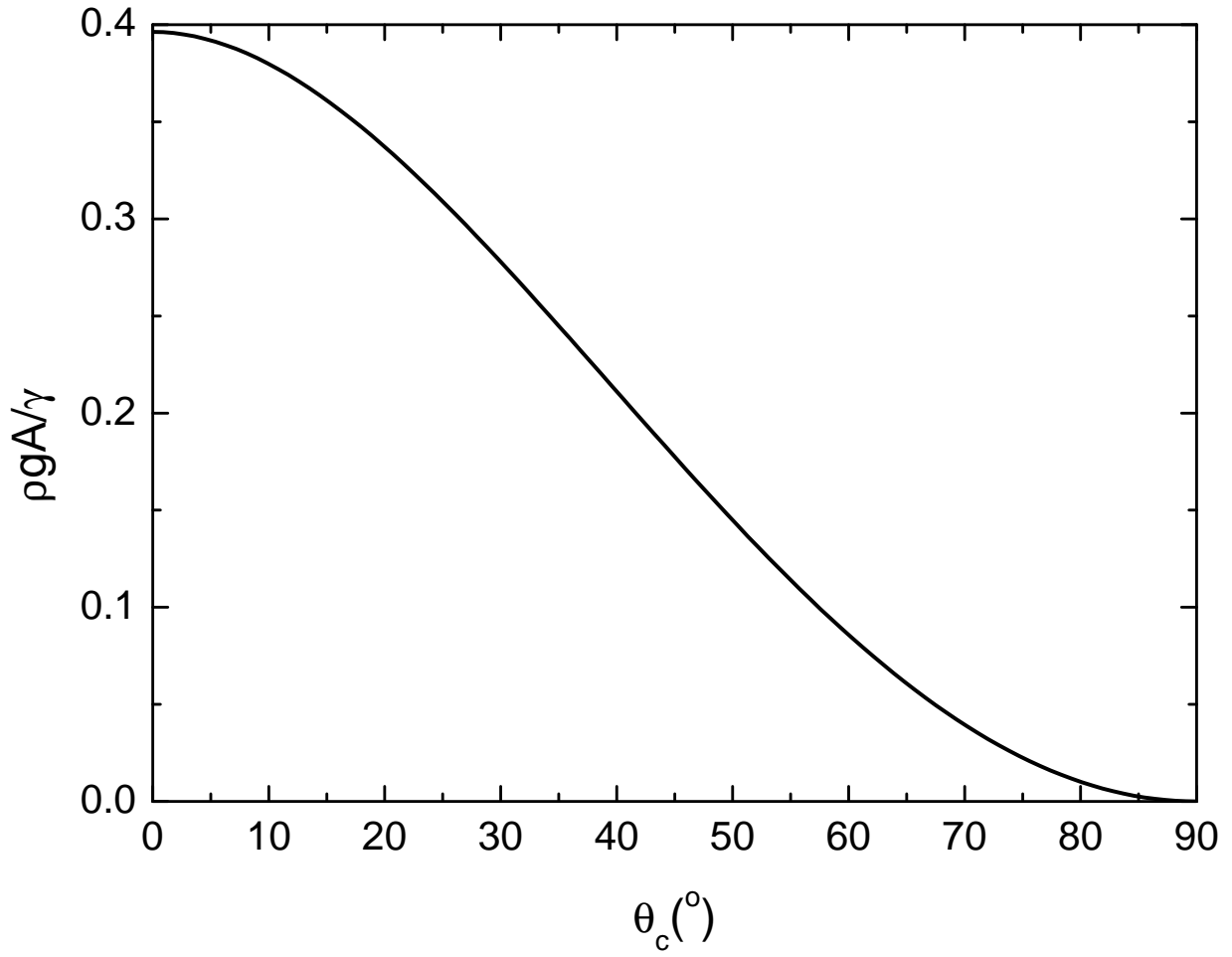


FIG. 14: Maximum top Plateau border area, normalised by square of capillary length, *vs* contact angle θ_c .